Supporting Information

Construction of Bimetallic FeCo-SA/DABCO Nanosheets by Modulating Electronic Structure for Improved Electrocatalytic Oxygen Evolution

Wenshuo Xie [a], Wei Deng [a,], Junbo Hu [a], Yuping Gai [a], Xiang Li [a], Jingjing Zhang [a], Dewu Long [b], Shanlin Qiao [c], Fei Jiang [a,]**

a School of Chemical and Environmental Engineering, Shanghai Institute of Technology, Shanghai, 201418, China
b Key Laboratory in Interfacial Physics and Technology, Shanghai Institute of Applied Physics, Chinese Academy of Sciences, Shanghai, 201800, China
c College of Chemistry and Pharmaceutical Engineering, Hebei University of Science and Technology, Shijiazhuang 050018, China

Material Characterization

Thermogravimetric analysis (Mettler Toledo) was carried out in the temperature range of 50°C-800 °C in air at a heating rate of 2 °C min^{-1}. The atomic ratio of the sample was determined using an energy dispersive X-ray spectroscope (EDS) and an inductively coupled plasma (ICP, Optima 2000DV). Powder XRD was performed using a PIXcel detector and an X'Pert PRO diffractometer (PA Nalytical) operating at 45 kV and 40 mA with Cu K radiation (= 1.541874). The BraggBrentano arrangement was used to capture data in the 2 range of 2080o at a scan speed of 4o min-1. On an ESCALAB 250Xi equipment with an Al K X-ray source, XPS characterisation was carried out (1486.6 eV).

An FEI Quanta 650 FEG microscope with an INCA 350 spectrometer was used for the SEM analysis (Oxford Instruments). On a Titan Themis TEM (Thermo Fisher Scientific) equipped with both probe and image Cs correctors and a Super-X EDS detector operating at 200 keV, TEM, STEM, and elemental mapping experiments were carried out. In situ heating studies were carried out in TEM mode with a double-tilt TEM heating holder (Lightning, DENS solutions), which allowed for extremely fast heating and cooling with little thermal drift. In a Bruker ICON SPM, conductive probes (NSC18, masch) were used in peak force mode to measure morphological and IV curves. Thermo-iCAPQc fisher's device was used to perform inductively coupled plasma atomic emission spectroscopy (ICP-AES). Nano Man VS Scope III was used to measure atomic force microscopes in knock mode (Digital Instrument).

Electrode Preparation and Electrocatalytic Tests

To make a mixed solution, 4 mg of electrocatalyst and 30µL of 5 wt % nafion were ultrasonically dispersed in 1 mL of ethanol and water (1:3) and ultrasonically dispersed for 30 minutes. The produced catalyst ink was loaded on a finely polished glassy carbon (GC) electrode with an exposed area of 0.07 cm^2, resulting in a noble metal loading density of around 0.28 mg cm^{-2} (4mg×5µL /3.14×0.15cm×0.15cm= 0.28mg cm^{-2}). The electrode was then dried naturally in the air at ambient temperature. At ambient temperature, all electrocatalytic studies were conducted in a three-electrode arrangement.

The working, counter, and reference electrodes were a catalyst-loaded GC, a Pt wire, and a saturated calomel electrode (SCE), respectively. The observed voltage against SCE was transformed to vs RHE using the following formula: $E_{RHE} = E_{SCE} + 0.231 + 0.0591$ pH. The apparent OER activity was evaluated using cyclic voltammetry (CV) at a 5 mV s1 scan rate, with an iR correction added to compensate for the voltage drop between the reference and working electrodes, which was determined using a single-point high-frequency impedance test. To minimize overestimation, the reduction branch of the CV curves was chosen to compare the performance of all the catalysts. At a constant current density of 10 mA cm^{-2}, the stability was tested.

CV experiments were performed in 1 M KOH (pH = 13.8) aqueous solution using a three-electrode system connected to an electrochemical workstation (CHI760E, Shanghai, China) at room temperature. Saturated calomel electrode (SCE) was denoted as the reference electrode and a platinum wire electrode was used as the counter electrode. CV tests with different scan rates from 20 to 100 $mV \cdot s^{-1}$ in the potential range of 0.9 - 1.0 V (νs. RHE) was performed to evaluate the electrochemical active surface area (ECSA) of the electrocatalysts. By plotting the capacitive currents (Janodic - Jcathodic) at 0.95 V (νs. RHE), the double-layer capacitance (C_{dl}) was equal to half of the slope. Then, the ECSA was computed by dividing the measured Cdl by the capacitance of a model catalyst over a unit surface area:

$$ECSA\ (cm^2) = Cdl/Cs = Cdl\ mF\ cm^{-2}/(40uFcm^{-2} \times 0.07cm^2)$$

(Cs is the capacitance of the corresponding smooth surface sample under the same conditions)

	C_{dl} (mF cm^{-2})	ECSA (cm^2)
Co-SA	3.77	6.60
Co-SA/DABCO	7.01	12.27
Fe-SA	1.945	3.40
Fe-SADABCO	2.18	3.81
FeCo-SA	9.15	16.01
FeCo-SA/DABCO	9.38	16.41

In order to obtain a deeper explanation of the enhanced OER activity of FeCo-SA/DABCO, the intrinsic OER activity can be obtained by calculating TOF according to Equation 1. TOF value indicates the amount of oxygen produced by the active sites of the catalyst per unit time. It is assumed that only metals are active sites in the catalyst, because they are non-metallic OER electrocatalysts that are more active.

$$TOF(\times 10^{-2}\, s^{-1}) = \frac{j(mA/cm^2) \times M_{w,catalys}(g/mol)}{F(C/mol) \times 4 \times m_{catalys}(mg/cm^2)} \qquad \text{Equation 1}$$

In Equation 1, j is the current density in a given overpotential, $M_{W,\ catalyst}$ is molar mass of the catalyst, F is Faraday constant (96485 C mol^{-1}), $m_{catalyst}$ is the loading of catalyst on the electrode.

Catalyst preparation:

To make a mixed solution, 4 mg of electrocatalyst and 30μL of 5 wt % nafion were ultrasonically dispersed in 1 mL of ethanol and water (1:3) and ultrasonically dispersed for 30 minutes. Then, using 5 μL of the combined solution, scatter it over a glassy carbon electrode with a diameter of 3 mm and dry it naturally for subsequent use.

DFT calculations:

Our total-energy computation used the plane-wave basis density functional theory pseudopotential approach and the Cambridge Sequential Total Energy Package CASTEP algorithm. [1] The Perdew–Burke–Ernzerhof GGA approach was used to represent the exchange and correlation potentials because the generalized gradient approximation GGA was more effective than the local-density approximation LDA in predicting the phase transition. [2]

The Vanderbilt-type ultrasoft pseudopotential was used to define the ionic potentials. A 750eV energy cutoff was applied, and a k-point sampling set of 5 × 5 × 1 was evaluated for convergence. The highest displacement was 5.0×10^{-4} Å with a force tolerance of 0.01 eV, an energy tolerance of 5.0×10^{-7} eV per atom, and a force tolerance of 0.01 eV. Each atom in the storage models was given the freedom to relax to the enthalpy minimum. The vacuum spacing along the direction was adjusted to 15 Å, which was adequate to keep the two adjoining pictures from colliding. FeCo-SA/DABCO and FeCo-SA surfaces have been constructed, and O_2, OH*, O*, OOH* groups have been absorbed on their surfaces.

The Volmer reaction (**equation S1**):

$$H_2O+M+e^- \rightarrow M\text{-}H^* + OH^-$$

The OER performances were evaluated by calculating the reaction free energy of each step:

$$\Delta G = \Delta E + \Delta E_{ZPE} - T\Delta S - eU$$

where the ΔE denotes the adsorption energy, ΔE_{ZPE} and ΔS are the changes of zero-point energy and entropy, and the temperature T is set to 300 K. U is the potential measured against normal hydrogen electrode (NHE) at standard conditions; e = 1 is the transferred charge for one-electron reactions. T = 300 K is considered.

The adsorbed intermediate free energy change ΔE_{ads} for steps 2–5 can be expressed as follows:

$$\Delta E_{OH^*} = E(OH^*) - E(^*) - [E(H_2O) - 1/2\, E(H_2))]$$

$$\Delta E_{O^*} = E(O^*) - E(^*) - [E(H_2O) - E(H_2)]$$

$$\Delta E_{OOH^*} = E(OOH^*) - E(^*) - [2E(H_2O) - 3/2\, E(H_2)]$$

Where E(*), E(OH*), E(O*) and E(OOH*) are the total energy of the clean surface and the adsorbed surface with three intermediates, respectively. $E(H_2O)$, $E(H_2)$ and $E(O_2)$ are the computed energies for the sole H_2O, H_2 and O_2 molecules, respectively.

In the alkaline environment, the overall OER process at the anode can be described by the following four-step associative mechanism (**equation S2**):

$$OH^- + * \rightarrow OH^* + e^-$$

$$OH^* + OH^- \rightarrow O^* + H_2O + e^-$$

$$OOH^* + OH^- \rightarrow OOH^* + e^-$$

$$OOH^* + OH^- \rightarrow O_2 + H_2O + e^-$$

where * and M* represent the active site and the adsorbed intermediate on the surface, respectively.

The Gibbs free energy change for steps 2–5 can be expressed as follows:

$$\Delta G_1 = \Delta G_{OH} - eU$$
$$\Delta G_2 = \Delta G_O - \Delta G_{OH} - eU$$
$$\Delta G_3 = \Delta G_{OOH} - \Delta G_O - eU$$
$$\Delta G_4 = 4.92[eV] - \Delta G_{OOH} - eU$$

where U is the potential measured against the normal hydrogen electrode at standard conditions. The theoretical overpotential can then be defined as **equation S3**:

$$\eta_{OER} = \max[\Delta G_1, \Delta G_2, \Delta G_3, \Delta G_4]/e - 1.23[V]$$

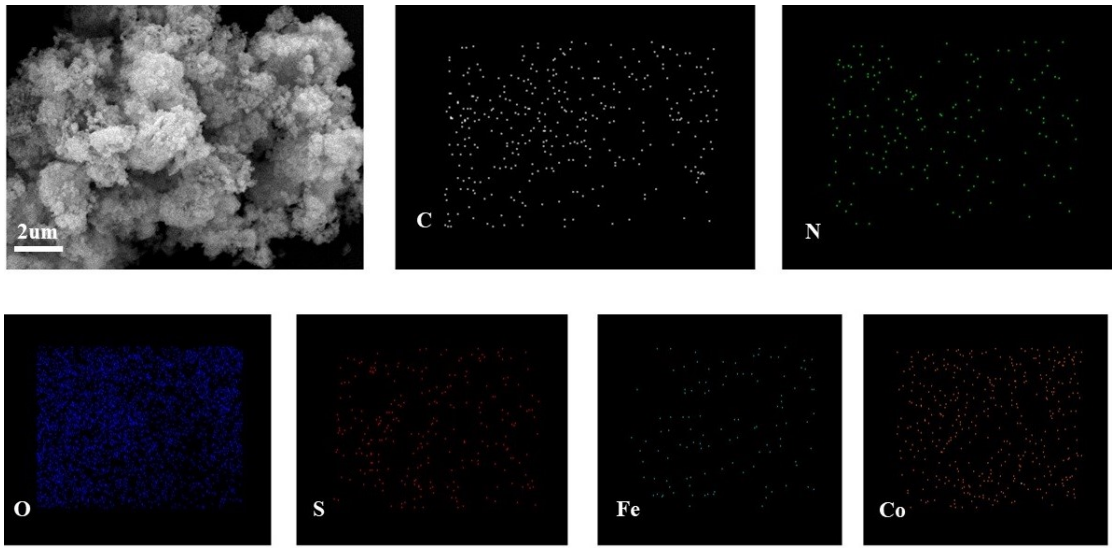

Fig S1. SEM EDS spectra of FeCo-SA/DABCO.

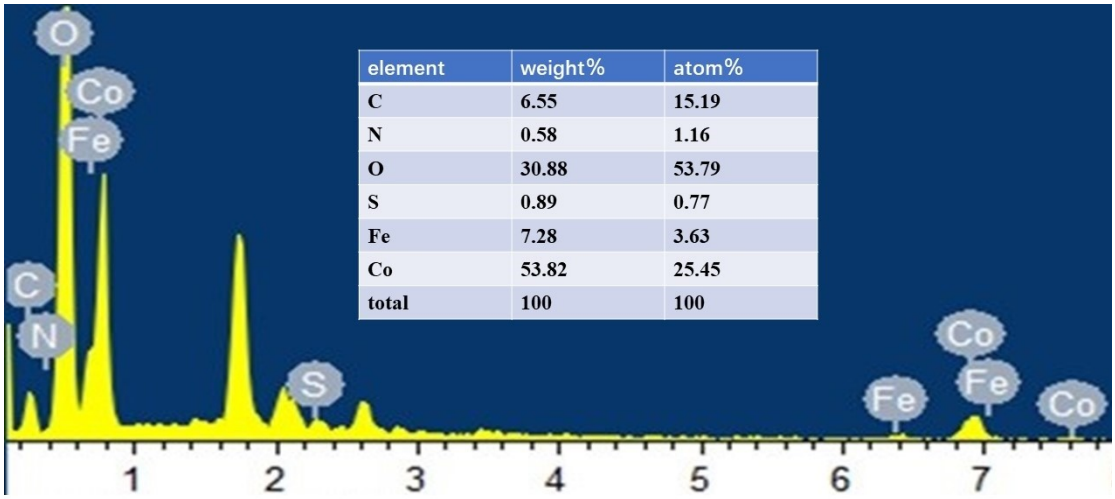

element	weight%	atom%
C	6.55	15.19
N	0.58	1.16
O	30.88	53.79
S	0.89	0.77
Fe	7.28	3.63
Co	53.82	25.45
total	100	100

Fig S2 EDS spectra of FeCo-SA/DABCO.

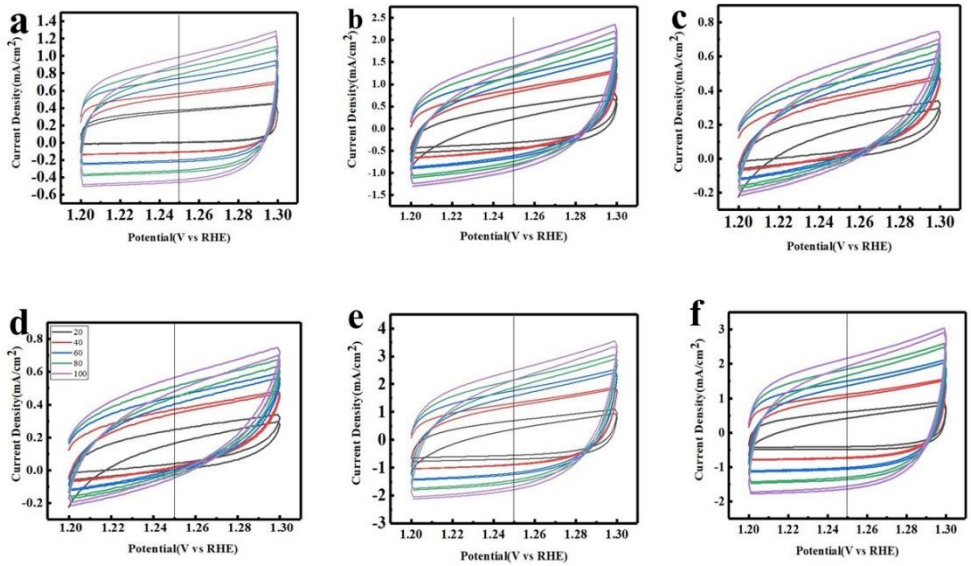

Fig S3 a. CV curves of Co-SA in the double layer region at different scan rates. b. CV curves of Co-SA/DABCO in the double layer region at different scan rates. c. CV curves of Fe-SA in the double layer region at different scan rates. d. CV curves of Fe-SA/DABCO in the double layer region at different scan rates. e. CV curves of FeCo-SA in the double layer region at different scan rates. f. CV curves of FeCo-SA/DABCO in the double layer region at different scan rates.

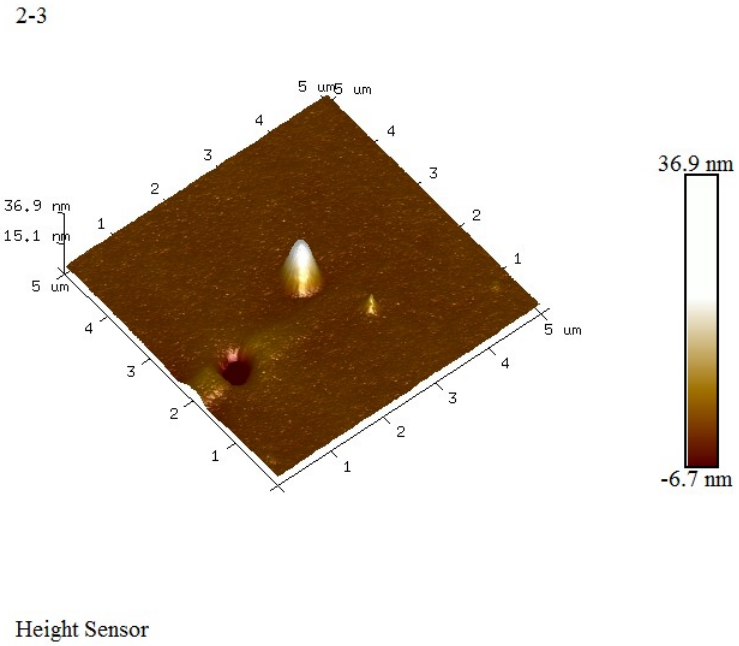

Fig S4 Atomic Force Microscope (AFM) Image.

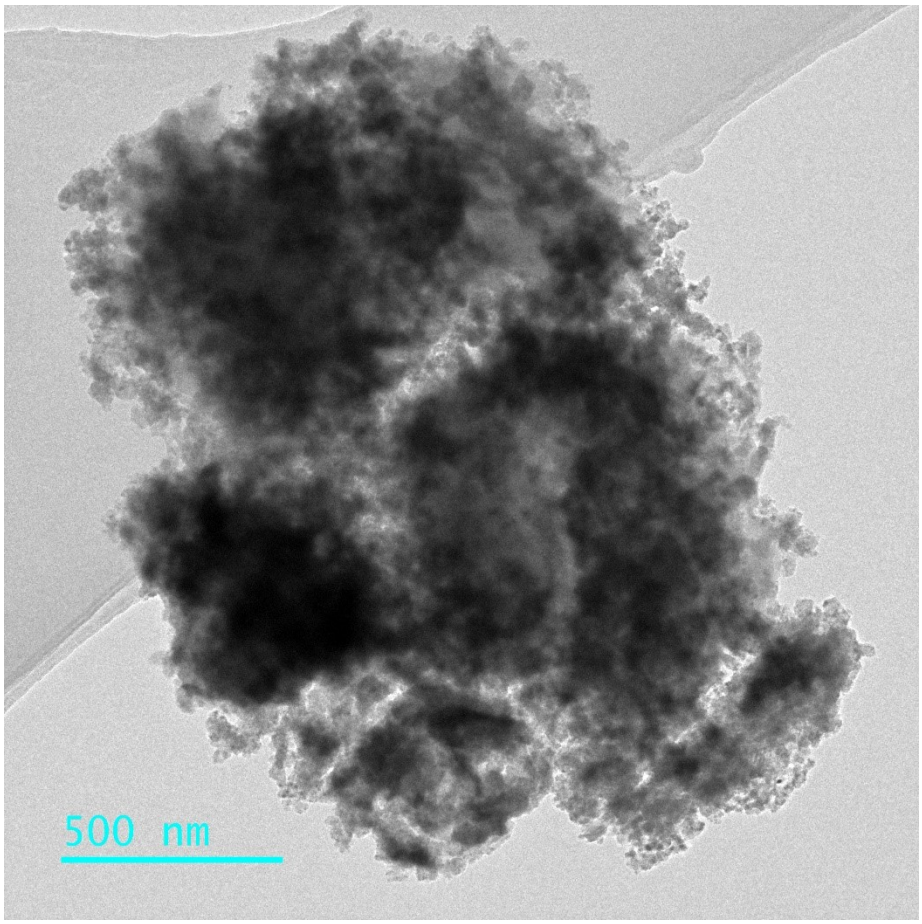

Fig S5TEM image of FeCo-SA/DABCO

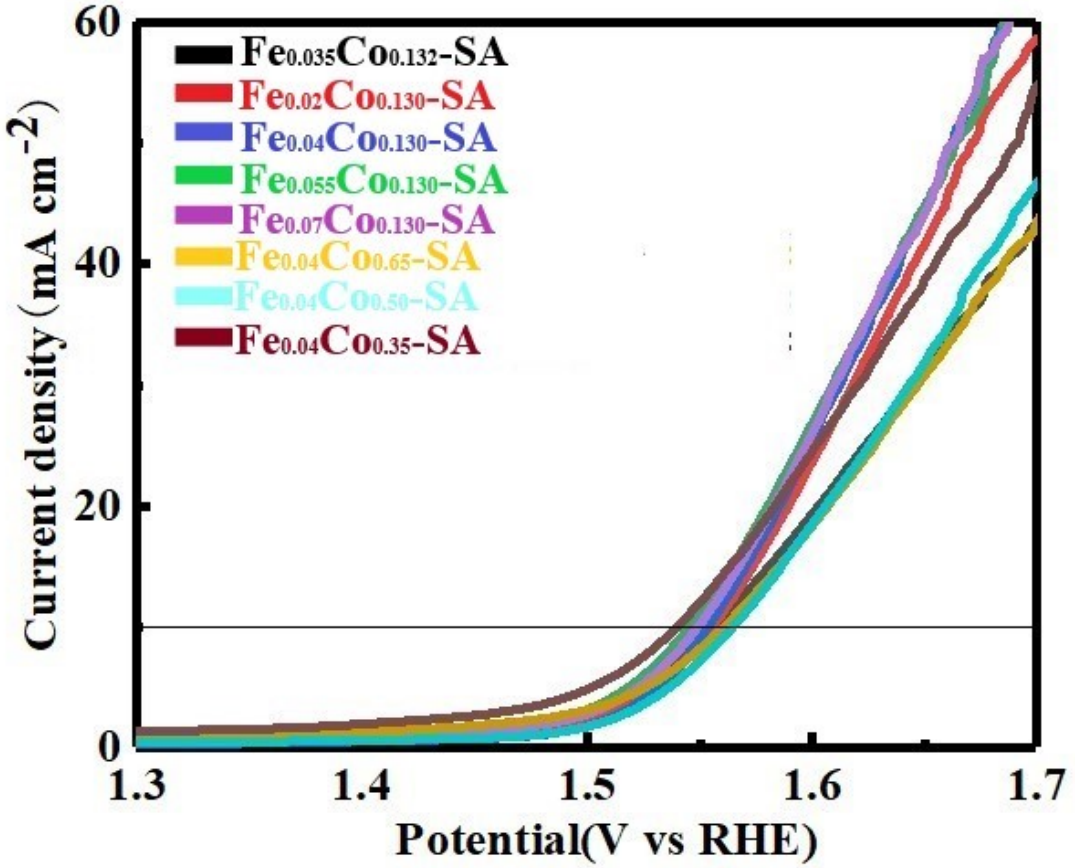

Fig S6 OER polarization curves of FeCo-SA in different ratios of cobalt nitrate hexahydrate and Ferric chloride hexahydrate.

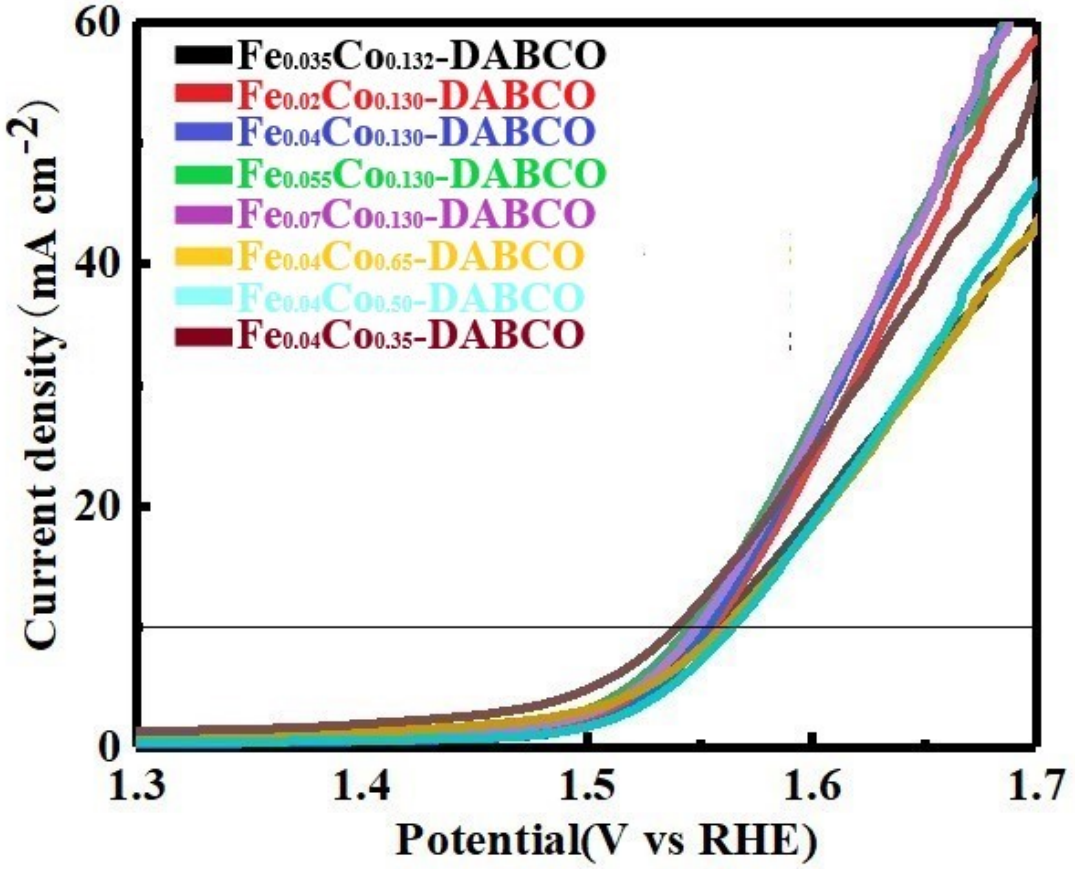

Fig S7 OER polarization curves of FeCo-DABCO in different ratios of cobalt nitrate hexahydrate and Ferric chloride hexahydrate.

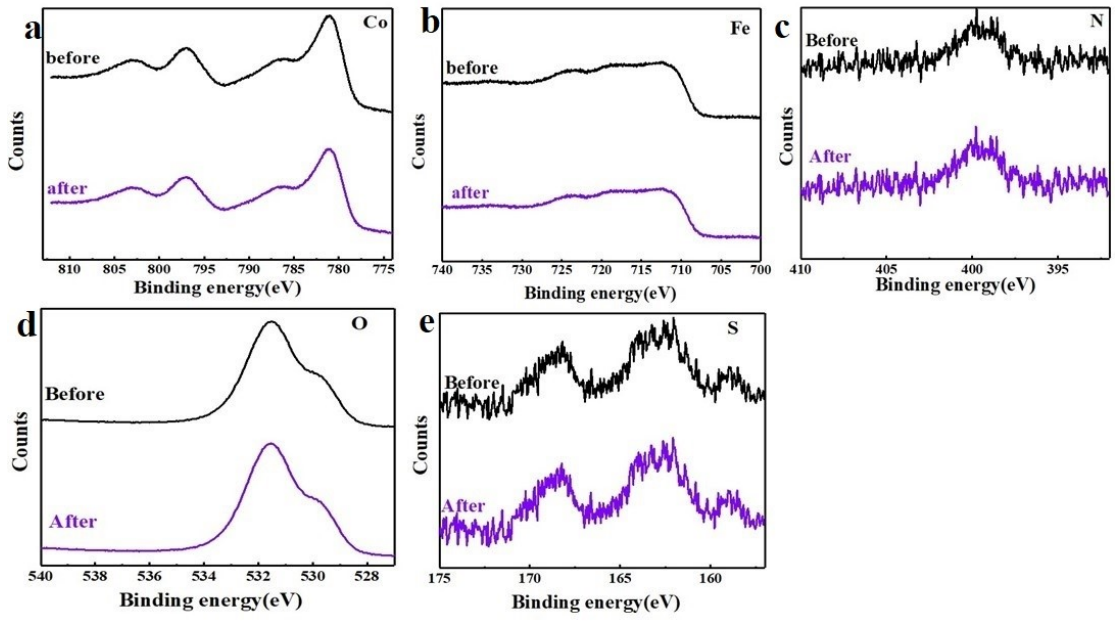

Fig S8 The XPS spectrum of FeCo-SA/DABCO before and after a) The high-resolution

of Co. b) The high-resolution of Fe. c) The high-resolution of N. d) The high-resolution of O. e) The high-resolution of S.

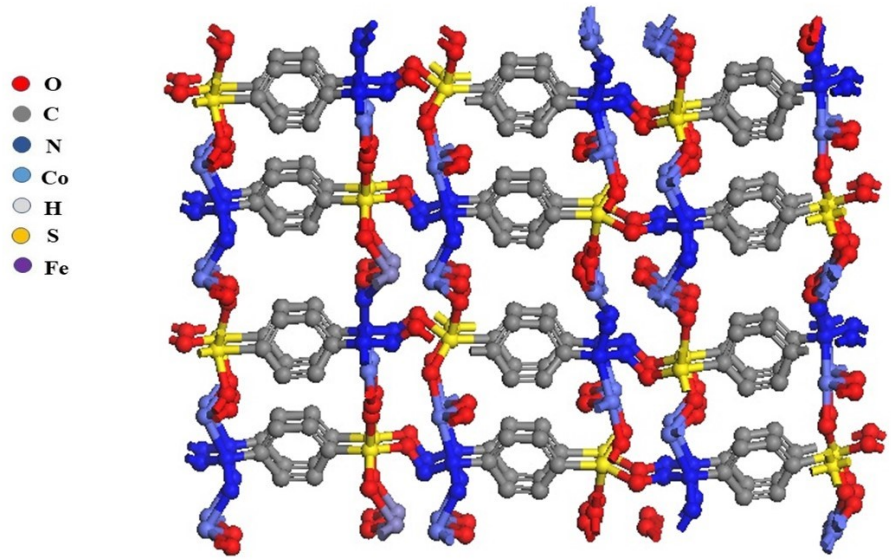

Fig S9 Structure diagram of FeCo-SA

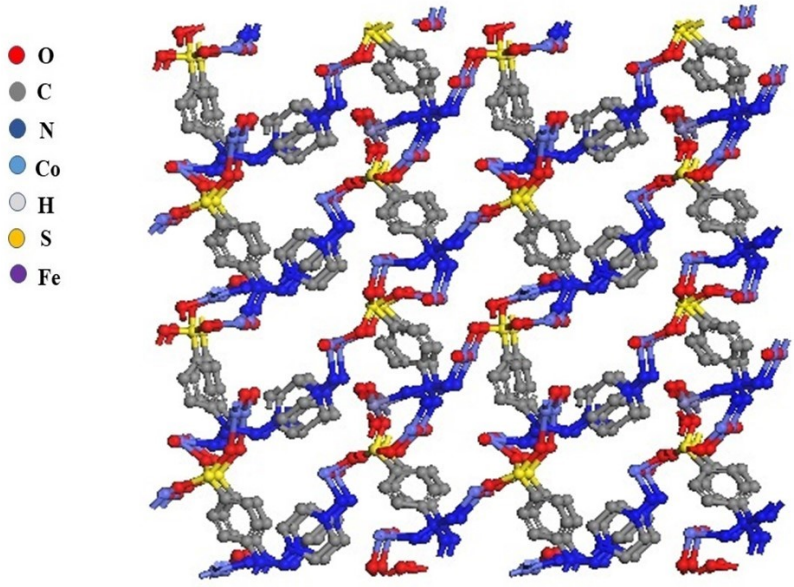

Fig S10 Structure diagram of FeCo-SA/DABCO.

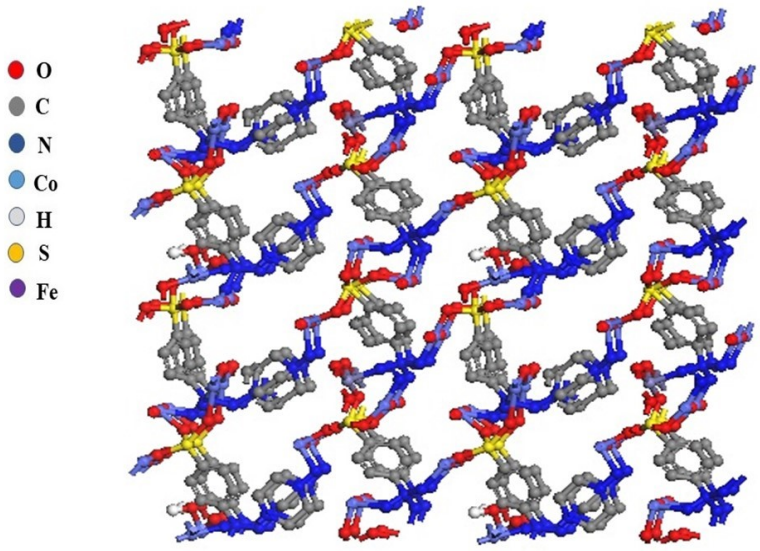

Fig S11 Structure diagram of FeCo-SA/DABCO (OH*)

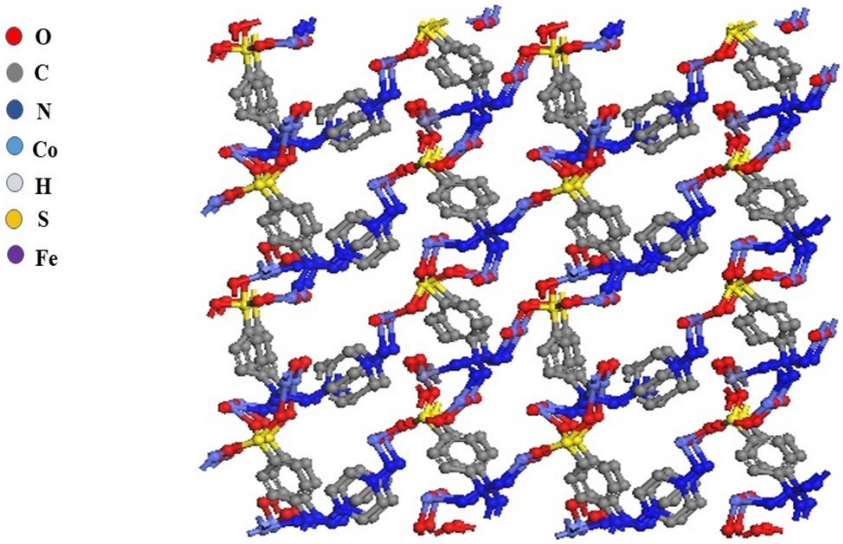

Fig S12 Structure diagram of FeCo-SA/DABCO (O*)

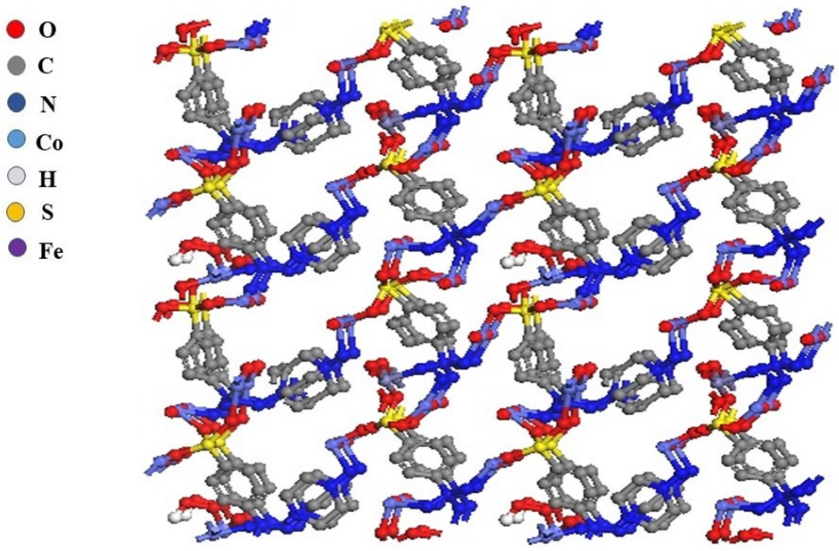

Fig S13 Structure diagram of FeCo-SA/DABCO (OOH*)

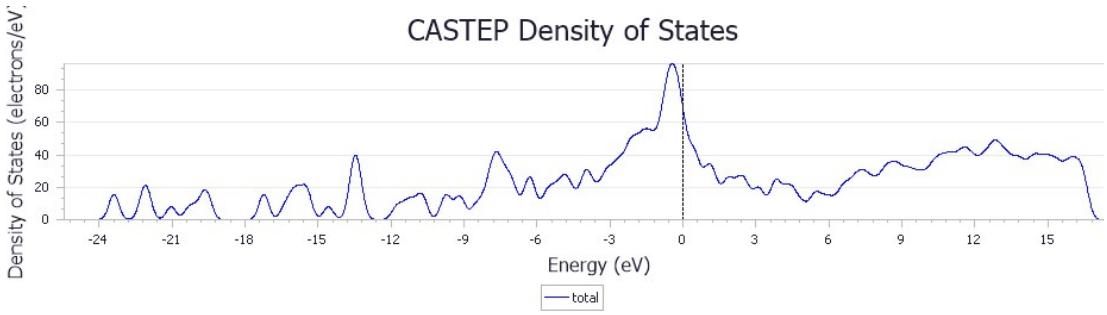

Fig S14 Calculated density of states (DOS) for FeCo-SADABCO

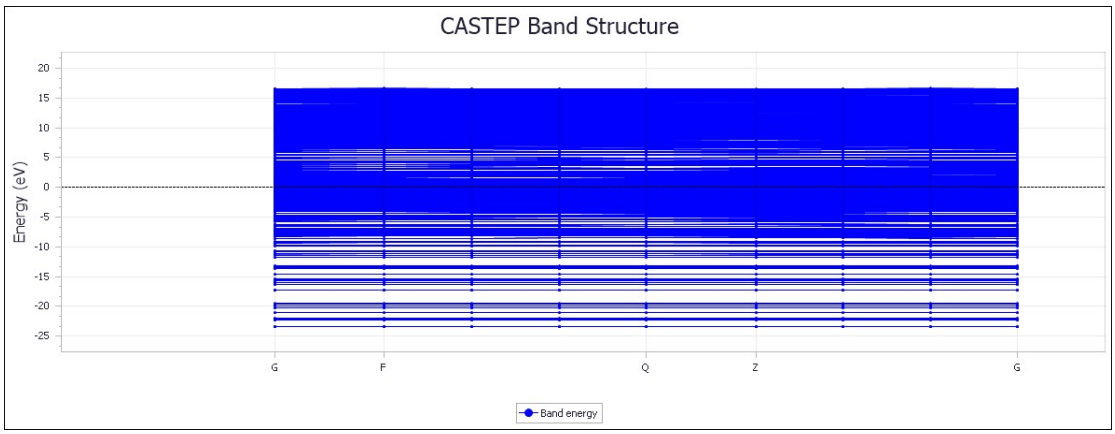

FigS15 Calculated band structure of FeCo-SADABCO

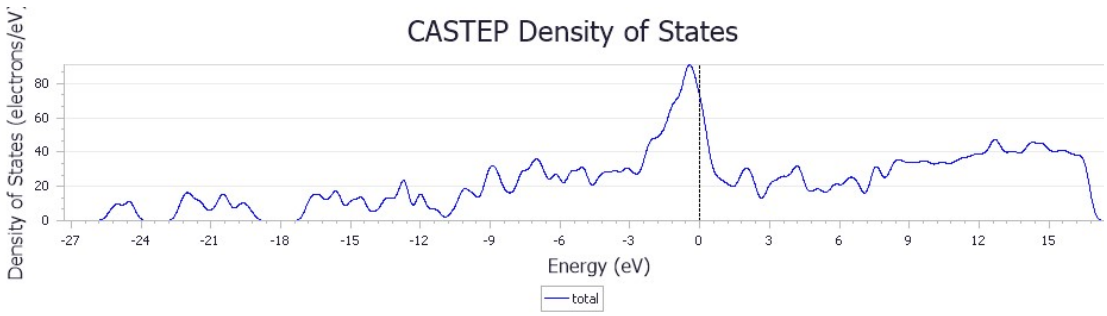

Fig S16 Calculated density of states (DOS) for FeCo-SA

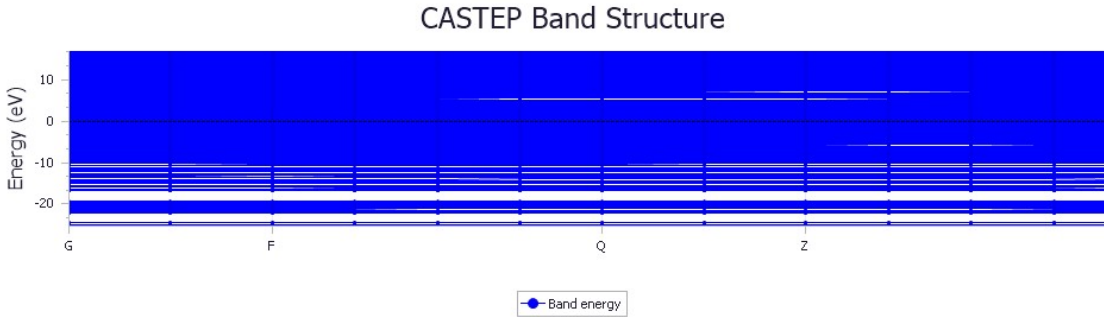

FigS17 Calculated band structure of FeCo-SA

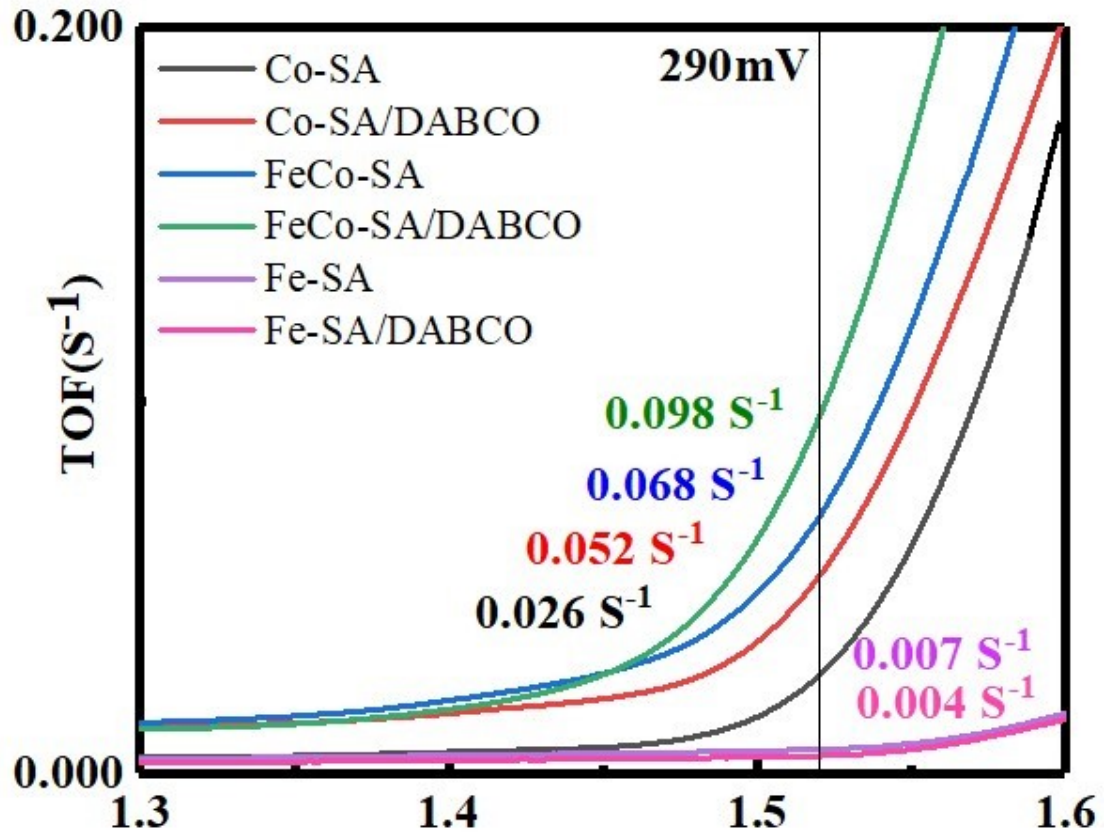

FigS18 TOF curves of FeCo-SA/DABCO, FeCo-SA, Co-SA/DABCO and Co-SA at the overpotential of 290 mV.

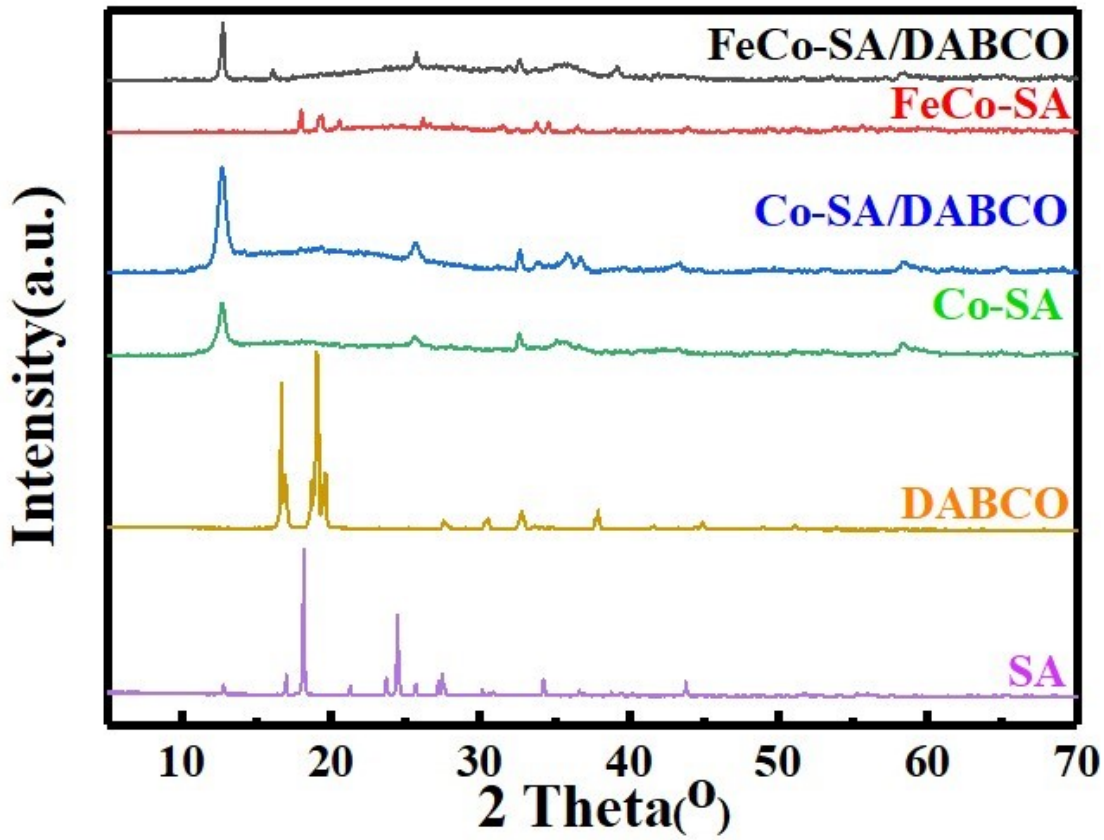

FigS19 XRD patterns of FeCo-SA/DABCO, FeCo-SA, Co-SA/DABCO, Co-SA, DABCO, and SA.

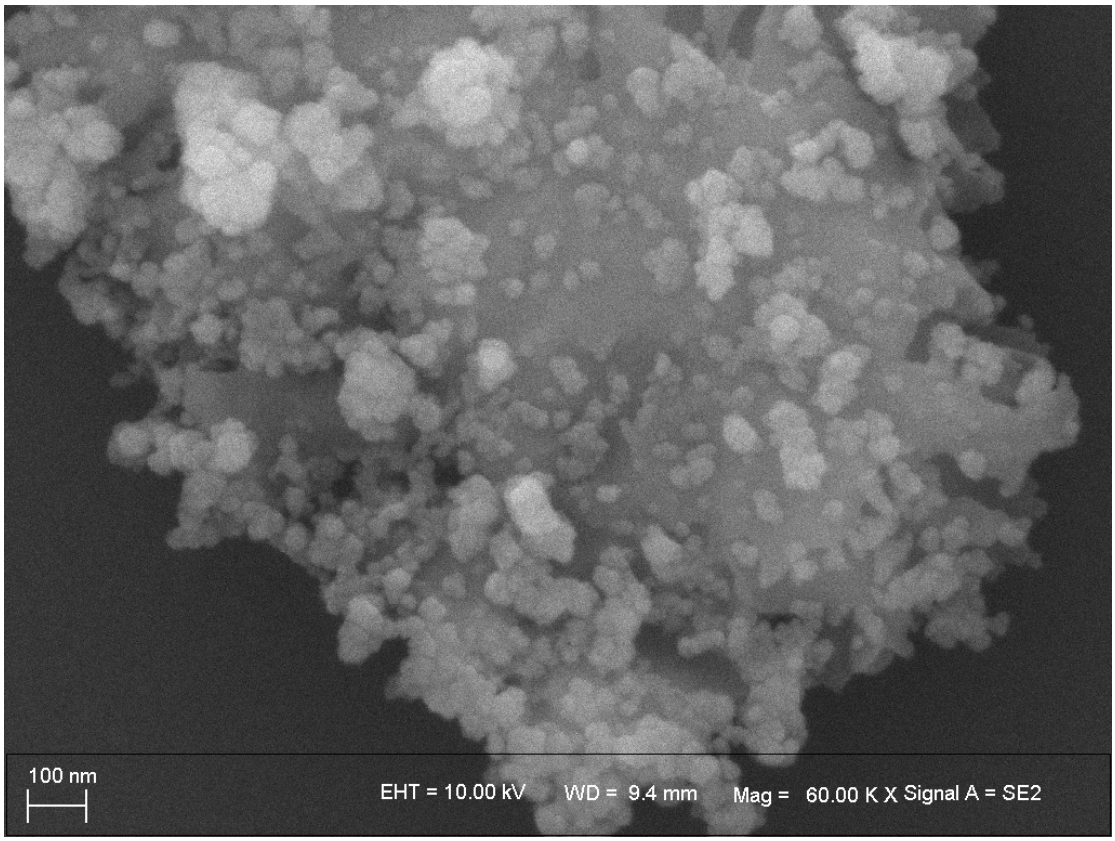

Fig. S20. SEM image of FeCo-SA/DABCO.

Reference

1 Y. C. Cheng, X. L. Wu, J. Zhu, L. L. Xu, S. H. Li, P. K. Chu, Optical properties of rocksalt and zinc blende AlN phases: First-principles calculations. Journal of Applied Physics, 2008, 103, 073707. https://doi.10.1063/1.2903138

2 K. Refson, P. R. Tulip, S. J. Clark, Variational density-functional perturbation theory for dielectrics and lattice dynamics. Physical Review B, 2006, 73. https://doi.10.1103/physrevb.73.155114